Infrared observations of Jovian aurora from Juno's first orbits: main oval and satellite footprints.

A. Mura[1], A. Adriani[1], F. Altieri[1], J.E.P. Connerney[2], S.J. Bolton[3], M.L. Moriconi[4], J-C. Gérard[5], W.S. Kurth[6], B.M. Dinelli[4], F. Fabiano[1,4], F. Tosi[1], S.K. Atreya[7], F. Bagenal[8], G.R. Gladstone[3], C. Hansen[9], S.M. Levin[10], B.H. Mauk[11], D.J. McComas[12], G. Sindoni[1], G. Filacchione[1], A. Migliorini[1], D. Grassi[1], G. Piccioni[1], R. Noschese[1], A. Cicchetti[1], D. Turrini[1,13], S. Stefani[1], M. Amoroso[14] and A. Olivieri[14]

1. INAF-Istituto di Astrofisica e Planetologia Spaziali, Roma, Italy
2. NASA Goddard Space Flight Center, Greenbelt, Maryland, USA
3. Southwest Research Institute, San Antonio, Texas, USA
4. CNR-Istituto di Scienze dell'Atmosfera e del Clima, Bologna / Roma, Italy
5. Universitè de Liège, Belgium.
6. University of Iowa, Iowa City, Iowa, USA
7. University of Michigan, Ann Arbor, Michigan, USA
8. University of Colorado, Boulder, Colorado, USA
9. Planetary Science Institute, Tucson, Arizona, USA
10. Jet Propulsion Laboratory, California Institute of Technology, Pasadena, California, USA
11. The Johns Hopkins University Applied Physics Laboratory, Laurel, Maryland, USA
12. PPPL, Princeton University, New Jersey, USA
13. UDA, Departamento de Fisica, Universidad de Atacama, Chile
14. Agenzia Spaziale Italiana, Roma, Italy

Corresponding Author: Alessandro Mura alessandro.mura@inaf.it

Abstract.

The Jovian Infrared Auroral Mapper (JIRAM) is an imager/spectrometer on board NASA/Juno mission dedicated to the study of the Jovian aurorae.

Here we present the first results of JIRAM's observations of the H_3^+ infrared emission with the *L* band imager channel, collected around the first Juno perijove (August 2016). These observations provide excellent spatial and temporal distribution of the Jovian aurora. They show the morphology of the main oval, the polar region, and the footprints of Io, Europa and Ganymede.

The extended "tail" downstream of Io persists for almost 5 hours after the passage of the satellite flux tube. Multi-arc structures of varied spatial extent appear in both the northern and southern main auroral ovals. Inside the main oval, intense, localized emissions are observed. In the southern polar region, a very evident circular region characterized by a strong depletion of H_3^+ emissions is partially surrounded by an intense emission arc. The southern

aurora is brighter than the north one in these observations, but similar and probably conjugate emission patterns are distinguishable in both polar regions.

Key points:

Tail of Io magnetic footprint longer than previously detected.

Identification of thin multiple arc structures in the northern and southern ovals, and of bright spots and depletion in the south pole

Filamentation of alternatively upward and downward current in the 0°-90° SIII sector in the north;

1 Introduction

The Jovian Infrared Auroral Mapper (JIRAM, Adriani et al., 2008, 2014, 2016) is an imaging spectrometer on board the Juno spacecraft, which started the prime mission around Jupiter on August 2016 (Bolton et al., 2017).

The JIRAM investigation was purposely designed to explore the Jovian aurorae and the planet's atmospheric structure, dynamics and composition. The main auroral oval emission is thought to be associated with upward field-aligned currents driven by the breakdown of corotation between the planet and the plasma sheet, partially supplied as neutral gas by Io's volcanic activity. It has been suggested that such breakdown occurs at equatorial magnetospheric distances from 15 to 40 RJ, and generates a global current system whose upward branch is associated with auroral precipitation (Cowley and Bunce, 2001; Hill, 2001). Outside of the main oval, signatures of electromagnetic interactions between Jupiter and its moons (particularly Io) are present (Connerney et al., 1993).

Emissions poleward of the main auroral oval are thought be connected to the outer magnetosphere, possibly related to a sector of the Dungey and Vasyliûnas cycle flows (Cowley et al., 2003; Grodent et al., 2003). In the UV, this region shows the highest temporal and spatial variability and this is where the largest differences in comparison to IR emission behaviors have been observed (Radioti et al., 2013).

Emission due to the H_3^+ ion is prominently observable in the JIRAM spectral range. Its main roto-vibrational band is around 2521 cm^{-1}, composed of more than 200 possible transitions in the range 3.0-5.0 μm; observation of the infrared emission of H_3^+ is mainly possible in a spectral interval (3.2 to 4.0 μm) where the solar and thermal radiance emitted by the planet are very low due to the intense atmospheric methane absorption band, resulting in a high auroral contrast against Jupiter's dark disk (Connerney and Satoh, 2000).

2 Data set

JIRAM combines two data channels (images and spectra) in one instrument. The optical design uses a reflecting telescope and a grating spectrometer in Littrow configuration. Two distinct focal plane detectors are used for imaging and spectroscopy. The aberrations in the telescope and spectrograph optical path are corrected with dioptric doublets. The instrument uses a dedicated de-spinning mirror to compensate for spacecraft rotation (1 or 2 rotations per minute). The instrument is designed to perform one acquisition, consisting of two 2D images in different spectral ranges/channels, and a 1D slit with full spectral resolution, every spacecraft rotation (currently 30 s). JIRAM can tilt its field of view (FoV) above or below the sub-spacecraft point, along the plane perpendicular to Juno spin axis, by delaying or anticipating the acquisition, which by default is taken at nadir. JIRAM cannot articulate its FoV in any other direction without turning the spacecraft.

The imager channel is a single detector (266 x 432 pixels) with two different filters (128 x 432 px each), separated by a 10-pixel wide, inactive strip. Of the two filters, one (*L* band, from 3.3 to 3.6 μm) is devoted to imaging H3+ emission and provides spatial context for the spectral observations. The pixel angular resolution is 0.01°. The FoV of the *L* band is 5.87° by 1.74 ° degrees. The spatial resolution, at the surface, varies with the spacecraft radial distance and it is

of the order of 100 km during most imaging activities. The other filter (*M* band, from 4.5 to 5 μm) is suitable for mapping the thermal structures of the atmosphere. Prior to observing Jupiter, a general calibration campaign was performed, including an assessment of pointing knowledge and accuracy and detector sensitivity, resulting in minor corrections of the pointing knowledge and sensitivity, revised to 2×10^6 counts s^{-1} / ($W\,m^{-2}\,sr^{-1}$).

JIRAM took more than 4000 images and spectra (Adriani et al., 2017, Dinelli et al., 2017) of Jupiter's aurorae and atmosphere prior to and immediately following the 1st Juno perijove pass (Aug. 27th 2016). In particular, more than 600 images of the filter-integrated radiance in the *L* band have been collected over the northern and southern aurorae, with an unprecedented spatial resolution and vantage point.

The JIRAM FoV is not able to cover the entire polar region in a single image during Juno's passage over the poles because the spacecraft is too close to Jupiter. However, JIRAM's field of view can be articulated with the scanning mirror to scan across most of the auroral features. These "tilted" images are organized in groups ("scans") of ~25 images each. Each image is a 1 second integration; images are acquired 30 seconds apart, so that a complete scan takes ~ 12 minutes to be performed. The resulting mosaic gives a comprehensive image of the aurora, and satellite footprints visible within the imaged area. Mosaics are assembled by processing the data to remove contamination (see section 3) and averaging the best available imagery where images overlap.

The northern aurora was observed from 08:24 to 11:51 UTC of August 27th 2016, with a total of 13 scans (one scan was incomplete due to partial data loss). The spatial resolution of these images varies from ~90 down to ~20 km. The southern aurora was observed from 15:06 to 19:51 UTC of August 27th 2016, with a total of 10 scans acquired. The spatial resolution of these images varies from ~50 km to ~130

3 Data processing

In some particular cases, the JIRAM *L* band images evidence significant contamination arising from strong signals present in the companion M band detector. The origin of the problem is not known at present but remains under study. Possible explanations include stray light within the optical system, and/or electron leakage on the detector. The same effect was evidently already present in JIRAM calibration observations of Earth's moon acquired during Juno's Earth flyby in 2013 (Adriani et al., 2016). However, the contamination was very faint and it remained unnoticed until data from Jupiter became available. In fact, this effect is relevant only for the *L*band detector, and it is observed only when the *M* band detector (which is beneath the *L* band one) receives a strong signal from Jupiter in its field of view (figure 1). The most unfavorable configuration occurs when looking JIRAM images the northern pole: in this case Jupiter fills the *M* band imager field of view. The intensity of the interference is higher than the radiance from H_3^+ emission, and it is therefore necessary to correct the data.

By analyzing the intensity and spatial variation of the interference observed when no real signal is present in the *L* band image FOV, it appears that the contamination is less intense for pixels that are distant from the *M/L* band border. The spatial variation of the interference signal has been fit with an exponential function with three free parameters:

$$N = C\, e^{-x/\lambda} + D \qquad (1)$$

where N is the noise count rate, C is an intensity value, λ is a scale length, D is a constant background value, and x is the distance, in pixels, from the L/M band border along the detector column. For each acquisition, and for each column of the image matrix, parameters C and D are variable. In contrast, the scale length is found to be almost constant in time and uniform along columns, with a value of about 20; but it too can be slightly tuned to improve the performance of the noise-removal algorithm. In principle, C is likely related to the intensity of the signal that is present in the M band channel. However, during scientific operations at Jupiter, JIRAM never takes both M and L images at the same time. Hence, a different approach is taken to find C and remove the constant background signal. We subtract the count rates of pixels in a subsequent image viewing the same surface location, and we assume that the signal has not changed between acquisitions 30 seconds apart, whereby D is canceled, and C can be obtained from:

$$N_1 - N_2 = C\left(e^{-x_1/\lambda} - e^{-x_2/\lambda}\right) \qquad (2)$$

This also assumes, as a necessary approximation, that C is constant in the same column on two subsequent images.

At the end of the procedure the background D is still not evaluated, but it is usually less than ~5 10^{-5} W m^{-2} sr^{-1} and does not significantly affect the data, since the instrument noise equivalent radiance (NER) is 10^{-5} W m^{-2} sr^{-1}. In addition, before every science image acquisition, JIRAM performs a "background frame" acquisition in the anti-nadir direction (dark sky image), and subtracts that from the targeted science image. This also allows removal of the focal plane's dark current generated by the spurious accumulation of thermal electrons, and the thermal emission generated by the instrument's inner walls and components.

In this way, it is possible to determine the parameters characterizing the noise contribution and partially remove the interference from the L band images (primarily northern aurora). The residual noise, and some artifacts arising from the noise removal procedure, are still visible in figure 4, but they do not affect the scientific interpretation of the data. We expect that turning off the JPEG compression currently employed to minimize telemetry resource usage will help in removing contamination from the data, because some artifacts are introduced by the JPEG compression as well, and not included in the corrections implemented with equation 2.

The measured radiance is mapped onto a reference surface 500 km above the 1 bar level using SPICE/NAIF routines and ancillary data (Acton, 1996). We chose this level as an average altitude, assuming most of the auroral emission originates in the vicinity (Grodent et al., 2001, Hiraki et al., 2008). The accuracy of the mapping to 500 km altitude is about as good as the projected pixel size (from 20 to 130 km, see above).

Juno's vantage point is close to the planet, and rapidly evolving along the spacecraft trajectory, so the emission angle also evolves rapidly. A higher emission angle implies a longer column for the emitted radiation. The image intensity is adjusted (multiplied by the cosine of the emission angle), assuming that radiance is constant along such column, to normalize the measured radiance to that coming from a vertical column. This also implies that there is no methane absorption above the H3+ emission region; in fact, the spectrometer measurements of the auroral region (made with the same viewing geometry of the imager) show that even where the methane emission is large, it is always superimposed to the H3+ spectrum, this indicates that

the two molecules either co-exist at the same altitudes or the methane layer is below the H3+ layer (Dinelli et al., 2017; Adriani et al., 2017; Moriconi et al., 2017). The image intensity is not the total H_3^+ emission, but only the segment in the filter passband.

4 Satellite footprints

Figures 2 and 3 show a total of 8 mosaic images of south aurora. White dashed lines show (from outside to inside): the magnetic mapping of the orbits of Io, Europa, Ganymede, and 30 Jupiter Radii (as a reference for the main oval) calculated using the VIP4 model (Connerney et al., 1998) combined with a model magnetodisc (Connerney et al., 1981). The white dots indicate the footprints of the positions of the moons (main spots, also indicated by letters I, E, G) during the observations.

The footprints (FP) of Io and Europa are very evident in the 270°-0° SIII longitude sector, and the agreement with the VIP4 model footprint locations is so good that we plot the VIP4 reference ovals only outside of the JIRAM image to avoid obscuration of the satellite related features. Unfortunately, for these images, the instantaneous satellite footprints lie outside of the mapped part of the aurora, and only the trailing tail is visible. In the case of Io, the distance between the calculated footprint location and the closest part of the visible tail is ~30° in longitude (~one hour of Jupiter-Io relative rotation). The tail extends for at least 90° in longitude with decreasing intensity but without appreciable change in its thickness (~500 km). The poleward edge is less sharp than the other one, as there is no auroral emission equatorward of the footprint of Io (i.e. no significant particle precipitation originating inside of Io's orbit). The brightness of Io's footprint decreases almost exponentially with a scale of ~2 hours (~70 degrees), and it appears that the Io's footprint tail is even longer if observed on unprocessed images (figure 1, panel *B*). Similar inferences apply to Europa's footprint; it has a similar intensity as Io's, but it is shorter and, being closer to the main oval, it is observable only for few tens of degrees in longitude. The footprint of Ganymede is visible, and it has two main spots (Bonfond et al., 2013a, 2013b, 2017) ~10 degrees above the predicted locations. It is visible particularly in figure 3; the two spots are visible in panels *A* and *D*; in panel *C* they form a segment and they are undistinguishable. In figure 2, it occurs to be too close to a stable, intense emission feature of the main oval, which covers the footprint. A very faint tail may be present.

Figure 4 shows four mosaic images of north aurora after data processing. The green dashed line is the statistical oval (UV) for that month as in Bagenal et al. (2014). The green spots are the expected locations of the Ganymede, Europa and Io footprints according to the statistical analysis of Hess et al. (2011). None of the main footprint spots are visible in the data; Io and Europa are very far from the FoV, and Ganymede is confused with the main oval emission. For this reason, no footprint model is added to the figure. Only a very tenuous part of the tail of Io may be visible close to 0°E, 80°N, but this feature is attributed to Io only because the positions given by Hess et al., (2011) are in correspondence with that feature.

5 Main oval

Earlier UV observations (Gerard et al., 1994; Ballester et al., 1996, Grodent et al., 2003) show that the shape of the statistical UV main auroral oval is quite repeatable in a Jupiter fixed frame, although second-order variations occur on time scales of tens of minutes, which is comparable to the time resolution of the mosaics (for this reason we prefer not to integrate all data into a

single image). Variations include intensifications (~50% increase) of main, stable emission features, and creations, movement and disappearance of minor structures.

Both in the UV and IR spectral ranges, the Jovian auroral morphology, on a global scale, is very similar and commonly divided into three main components: 1) outer emissions (including the footprints), 2) main oval (or main emission) and 3) polar emissions (e.g. Satoh and Connerney, 1999a,b, Clarke et al. 2004, Radioti et al., 2013, Grodent 2015). UV auroral features mainly result from inelastic collisions of energetic electrons of magnetospheric origin with atmospheric molecular hydrogen, whereas IR auroral emissions are due primarily to thermal emissions from the H3+ molecular ion at altitudes above the Jovian homopause.

As in UV images (Grodent et al., 2003, Gladstone et al., 2017, Connerney et al., 2017), the main oval (both south and north ones) shows a narrow single arc in about one half of the oval, and multiple arcs plus broad diffuse emissions in the other half. In the infrared, it seems that, in the south, the broad region is between 270° and 0°, and a single arc is visible between 90° and 180° (however, 180°-270° is not covered in the south pole). However, as Juno's UV and IR images were not obtained at the same instant in time, during this perijove pass, we urge caution in direct comparison of the two. In the north, a main single arc (plus some parallel secondary arcs) is visible between 150° and 270° (magnetic longitudes), and the broad, multi-arc region covers the remaining part. In both hemispheres, the diffuse region shows multiple structures of coherent pattern. The northern aurora, for example, shows concentric arcs of similar morphology (~200 km thick) placed from the main oval poleward, so that one might infer that such a region is still magnetically conjugate with the southern aurora, i.e., closing across the magnetic equator. These structures may correspond to a filamentation of alternatively upward and downward current, in contrast to the simple paradigm of a single current loop connecting the magnetosphere and the ionosphere. Part of the remaining region might map to the outer magnetosphere, possibly related to a sector of the Dungey and Vasyliûnas cycle flows (Cowley et al., 2003; Grodent et al., 2003).

The unprecedented spatial resolution of the JIRAM IR observations helps constrain the thickness of the single arc region, which is found to be uniformly equal to 500 km for the south and 700 km for the north. This could help constraining the theoretical models such as that of Cowley and Bunce (2001), as discussed in Grodent et al. (2003).

The southern aurora appears significantly brighter at the time of observation (~50% higher intensity), as found in the spectrometer measurements (Adriani et al., 2017; Dinelli et al., 2017). Three or four diffuse emission spots, placed at 0° System III west longitude and outside the main oval in the south, are visible in the spectrometer data as well, and can be linked with similar features in the north aurora at 0° longitude.

The local time variation of the emission is not easy to quantify at present. Because of the configuration of JIRAM FoV and Juno orbit, observation of the dawn sector is correlated with low emission angle. Even if the data are corrected for the emission angle variations (see section 3), an unavoidable observation bias could remain. If we compare the emission for a given feature at different local times, there are some indications that the emission decreases after dawn and the increases again at noon local time, in agreement with observations reported by Adriani et al. (2017). A specific detailed analysis is needed to confirm this.

6 Summary, conclusions and future perspectives

JIRAM collected ~ 6 Gb of data before and after PJ1,, and the investigation was extremely successful in addressing its primary scientific objectives. In particular, the north and south aurorae have been mapped by both the spectrometer and the *L* band imager channel. High-resolution images of both poles show very thin structures (few hundreds of km) that have the tendency to remain compact within time scales of the order of 1 hour. Although the footprints of Europa and Io fell outside the JIRAM FoV in the images acquired in this first periapsis pass, their tails were clearly detected, with a structure both well defined (few hundreds of km width) and extended along the satellite L-shell (at least 180 degrees longitude, probably more). The footprint of Ganymede, and possibly its tail, is visible in the southern aurora.

Inside the main oval, two different types of structures are observed: multi-arc structures, and bright or dark spots. The multi-arc structures appear both in the northern and southern pole close to the 0° meridian (in the north, such arcs are very thin) and we interpret these structures, similar in shape as the main oval, as magnetically conjugate features, connecting across the magnetic equator. In particular, the north aurora filaments may be interpreted as alternatively upward and downward current.

In the north, inside main oval, small, bright, transient spots are observed with persistence lifetime of hours or less. Outside of the main oval, bright spots are clearly seen close to 0° longitude. There may be signatures of plasma injections, and they are substantially stable in a SIII reference.

In the south, a very evident circular region, almost at the geographical pole, shows a strong depletion of H_3^+ emissions. This feature it is partially surrounded by a very bright arc, characterized by significant intensity variations.

JIRAM did not collect data on PJ 2 and PJ 3, as a result of the interruption of normal spacecraft operations, but during PJ4 JIRAM returned to normal science operations, to continue spectrometry and imagery of the aurorae.

References

Acton, C.H., (1996). Ancillary data services of NASA's navigation and ancillary information facility. Planet. Space. Sci. 44 (1), 65-70

Adriani A, Coradini A, Filacchione G, Lunine JI, Bini A, Pasqui C, Calamai L, Colosimo F, Dinelli BM, Grassi D, Magni G, Moriconi ML, Orosei R. (2008). JIRAM, the image spectrometer in the near infrared on board the Juno mission to Jupiter. Astrobiology. 2008 Jun;8(3):613-22. doi: 10.1089/ast.2007.0167.

Adriani A., G. Filacchione, T. Di Iorio, D. Turrini, R. Noschese, A. Cicchetti, D. Grassi, A. Mura, G. Sindoni, M. Zambelli, G. Piccioni, M.T. Capria, F. Tosi, R. Orosei, B.M. Dinelli, M.L. Moriconi, E. Roncon, J.I. Lunine, H.N. Becker, A. Bini, A. Barbis, L. Calamai, C. Pasqui, S. Nencioni, M. Rossi, M. Lastri, R. Formaro, A. Olivieri (2014), JIRAM, the Jovian Infrared Auroral Mapper. Space Sci. Rev., DOI 10.1007/s11214-014-0094-y.

297 Adriani, A.; Mura, et al., (2016), Juno's Earth flyby: the Jovian infrared Auroral Mapper
298 preliminary results, Astrophysics and Space Science 361(8).

299 Adriani et al., this issue

300 Bagenal F.,A. Adriani, F. Allegrini, S.J. Bolton, B. Bonfond, E.J. Bunce, J.E.P. Connerney, S.W.H.
301 Cowley, R.W. Ebert, G.R. Gladstone, C.J. Hansen, W.S. Kurth, S.M. Levin, B.H. Mauk, D.J. McComas,
302 C.P. Paranicas, D. Santos-Costa, R.M. Thorne, P. Valek, J.H. Waite, P. Zarka (2014),
303 Magnetospheric Science Objectives of the Juno Mission, Space Sci Rev, DOI 10.1007/s11214-
304 014-0036-8.

305 Ballester, G. E., et al. (1996), Time-resolved observations of Jupiter's far- ultraviolet aurora, Science,
306 274, 409–412.

307 Bolton S.J., et al. (2017) Science

308 Bonfond, B., S. Hess, J.-C. Gérard, D. Grodent, A. Radioti, V. Chantry, J. Saur, S. Jacobsen, J.T.
309 Clarke, (2013a) Evolution of the Io footprint brightness I: Far-UV observations, Planetary and
310 Space Science, 2013, 88, 64

311 Bonfond, B., S. Hess, F. Bagenal, J.-C. Gérard, D. Grodent, A. Radioti, J. Gustin, and J. T. Clarke,
312 (2013b) The multiple spots of the Ganymede auroral footprint, GEOPHYSICAL RESEARCH
313 LETTERS, VOL. 40, 4977–4981, doi:10.1002/grl.50989, 201

314 Bonfond, B., Grodent, D., Badman, S. V., Saur, J., Gérard, J. C., Radioti, A. (2017). Similarity of the
315 Jovian satellite footprints: spots multiplicity and dynamics. Icarus.

316 Connerney, J. E. P., M. H. Acuna and N. F. Ness, "Modeling the Jovian current sheet and inner
317 magnetosphere", *J. Geophys. Res.*, 86, 8370 - 8384, 1981.

318 Connerney, J. E. P., R. Baron, T. Satoh, and T. Owen, "Images of excited H_3+ at the Foot of the Io
319 Flux Tube in Jupiter's atmosphere", *Science*, 262, 1035 - 1038, 1993.

320 Connerney, J. E. P., M. H. Acuña, N. F. Ness, and T. Satoh (1998) New models of Jupiter's magnetic
321 field constrained by the Io flux tube footprint, J. Geophys. Res., 103(A6), 11,929–11,939.

322 Connerney, J. E. P., and T. Satoh, "The H_3+ ion: A remote diagnostic of the Jovian
323 magnetosphere", *Phil. Trans. R. Soc. Lond.* A, 358, 2471 - 2483, 2000.

324 Connerney, J. E. P., et al., Science (2017)

325 Cowley, S. W. H., and E. J. Bunce (2001), Origin of the main auroral oval in Jupiter's coupled
326 magnetosphere-ionosphere system, Planet. Space Sci., 49, 1067–1088.

327 Cowley, S. W. H., E. J. Bunce, T. S. Stallard, and S. Miller (2003), Jupiter's polar ionospheric flows:
328 Theoretical interpretation, Geophys. Res. Lett., 30(5), 1220, doi:10.1029/2002GL016030.

329 Dinelli et al., this issue.

330 Gérard, J.-C., V. Dols, R. Prange, and F. Paresce (1994), The morphology of the north Jovian
331 ultraviolet aurora observed with the Hubble Space Telescope, Planet. Space Sci., 42, 905–917.

Gérard, J.C., Saglam, A., Grodent, D., Clarke, J.T., 2006. Morphology of the ultraviolet Io footprint emission and its control by Io's location. Journal of Geophysical Research 111, A04202.

Gladstone, R., et al, this issue

Grodent, D., Waite Jr., J. H., and Gérard, J.-C. (2001): A self-consistent model of the Jovian auroral thermal structure, J. Geophys. Res., 106(A7), 12 933–12 952.

Grodent, D., J. T. Clarke, J. Kim, J. H. Waite Jr., and S. W. H. Cowley (2003), Jupiter's main auroral oval observed with HST-STIS, J. Geophys. Res. Lett., 180, 1389, doi:10.1029/20003JA009921.

Hess, S.L.G., B. Bonfond, P. Zarka, D. Grodent, (2011), Model of the Jovian magnetic field topology constrained by the Io auroral emissions. J. Geophys. Res. 116, 5217.

Hill, T. W. (2001), The Jovian auroral oval, J. Geophys. Res., 106, 8101–8107.

Hiraki, Y., Tao, C., 2008. Parameterization of ionization rate by auroral electron precipitation in Jupiter. Ann. Geophys. 26, 77–86.

Moriconi et al., this issue.

Radioti, A., M. Lystrup, B. Bonfond, D. Grodent, and J.-C. Gérard (2013) Jupiter's aurora in ultraviolet and infrared: Simultaneous observations with the Hubble Space Telescope and the NASA Infrared Telescope Facility J. Geophys. Res, 118, 2286–2295, doi:10.1002/jgra.50245.

Satoh, T.,and J. E. P. Connerney, "Jupiter's H_3+ emissions viewed in corrected Jovimagnetic coordinates", *Icarus*, 141, 236 - 252, 1999.

Satoh, T.,and J. E. P. Connerney, "Spatial and temporal variations of Jupiter's H_3+ emissions deduced from image analysis", *Geophys. Res. Lett.*, 26, 1789 - 1792, 1999.

Acknowledgements

We thank the Italian Space Agency, ASI, for support of the JIRAM contribution to the Juno mission.

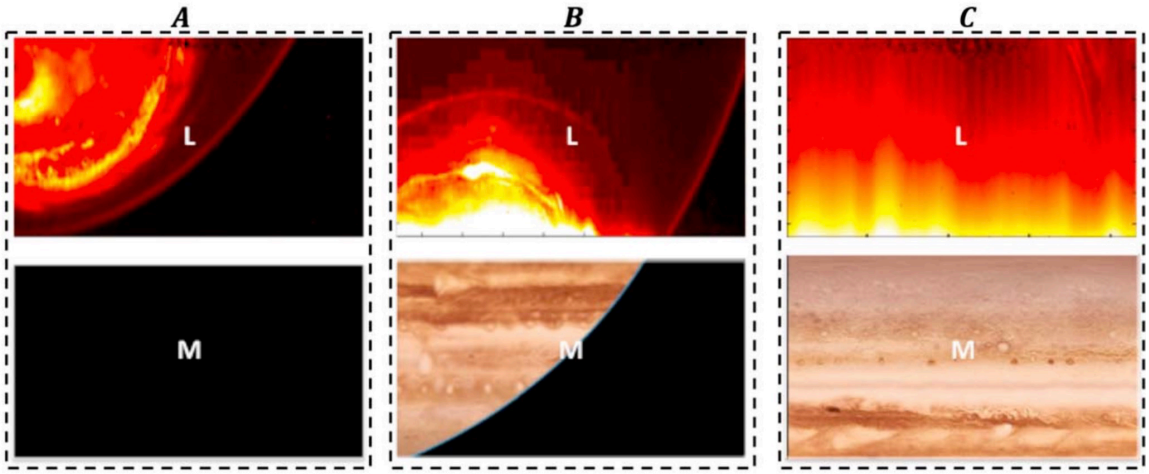

355

Figure 1. Examples of L band data and contamination (top panels) function of M channel pointing (bottom, graphic art). A: South Aurora, very low contamination, M band FoV is pointing towards empty space. B: South Aurora, medium contamination in the bottom of the image; M band FoV is partially filled by Jupiter. C: North Aurora, very high contamination, M band FoV is completely filled by Jupiter.

356

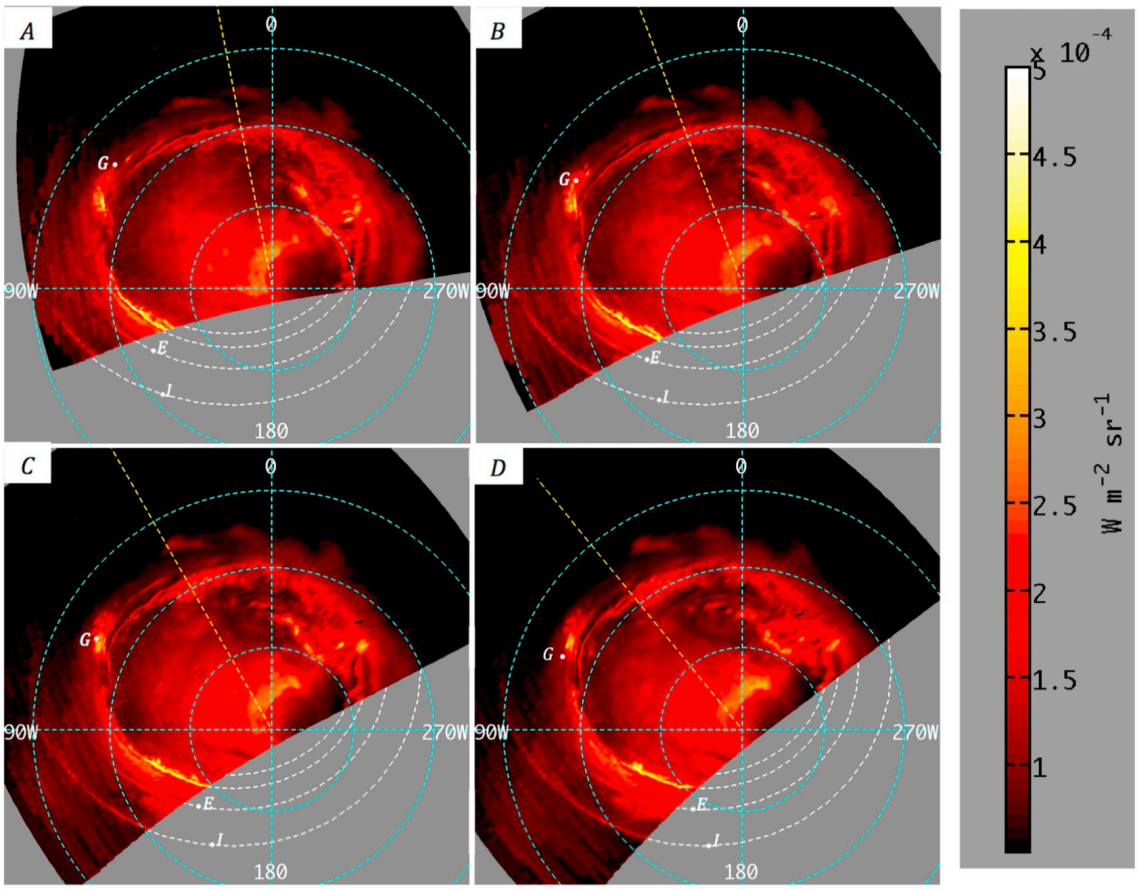

Figure 2 Mosaic maps of emission (3.3-3.6 µm average radiance) from south aurora taken on August, 27th 2016. Cyan dashed circles are parallels at 80°, 70° and 60° latitude; longitudes are SIII; Sun direction is indicated by yellow line. White dashed lines are footprints of moons and 30 RJ according to VIP4 model (see text for explanations). Starting UTC times of observations are: 17:53:59 (panel A); 18:09:21 (B); 18:24:43 (C); 18:40:36 (D). White points are predicted footprint positions indicated by letters I, E and G.

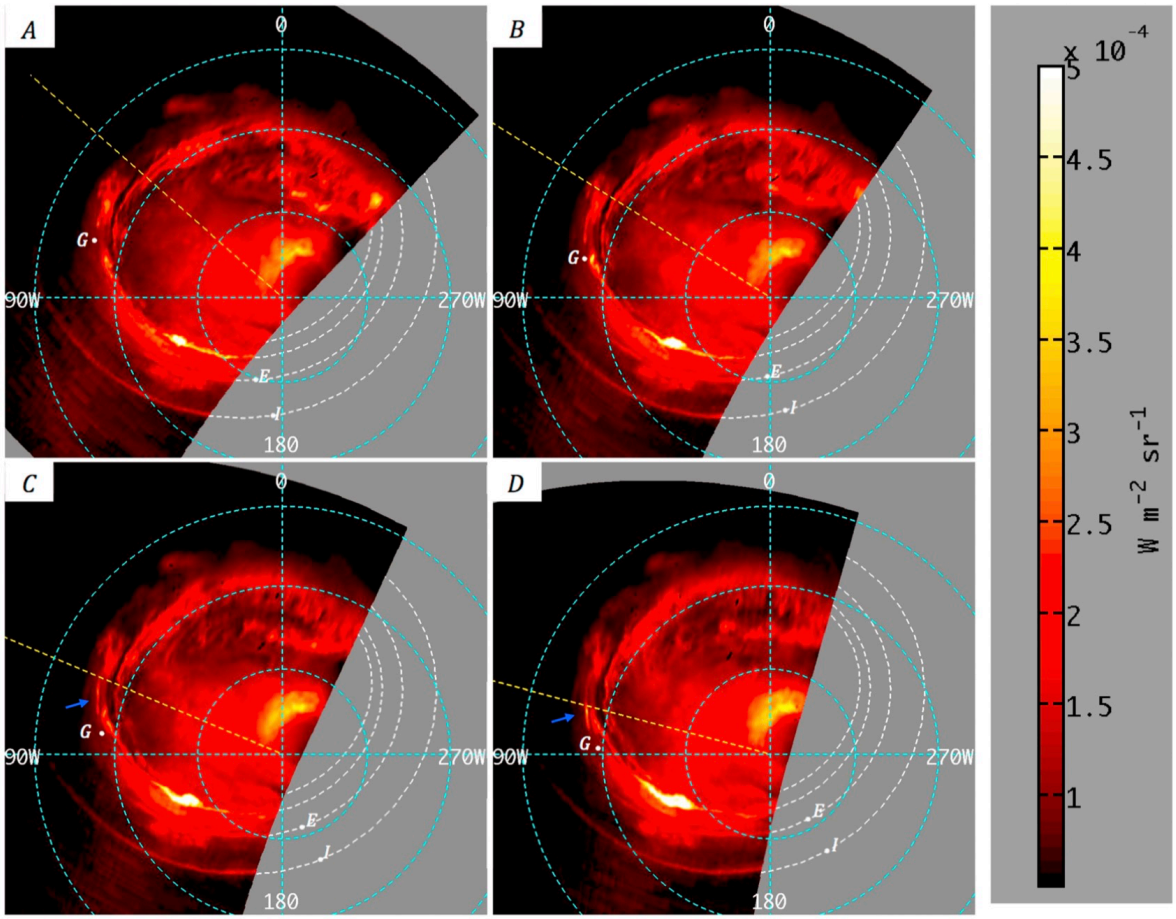

Figure 3 Same as figure 2, starting UTC times of observations are: 18:55:58 (panel A); 19:11:20 (B); 19:26:42 (C); 19:41:34 (D). A blue arrow (panel D only) indicates the feature that is identified as Ganymede footprint.

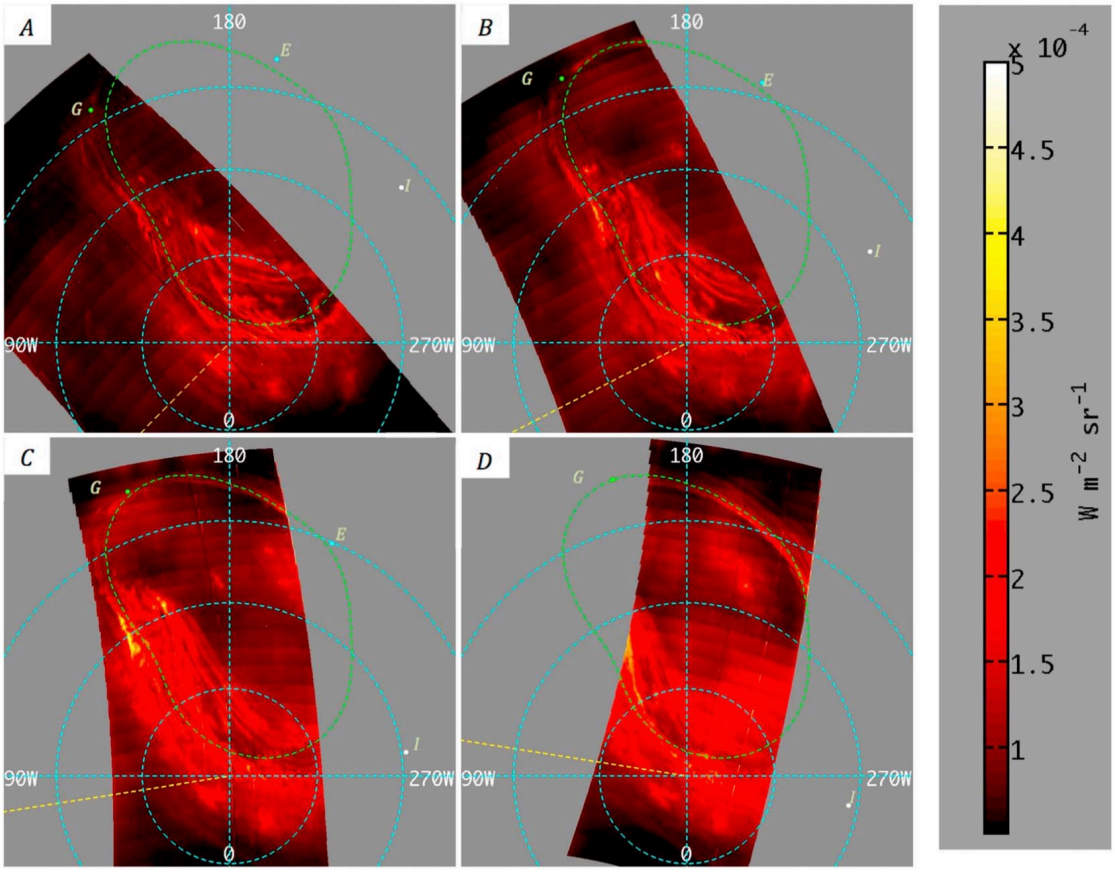

Figure 4. Same as figure 2, for north aurora. Green dashed line: statistical oval for that month as in Bagenal et al. (2014). Green spots are (clockwise) statistical positions of Ganymede, Europa and Io footprints (Hess et al., 2011; Europa FP position at the time of panel D was not available). Starting times of observations are: 08:53:58 (panel A), 09:24:11 (B), 09:54:23 (C), 10:24:05 (D).